International Journal of Innovative Environmental Studies Research 14(2):255-276 April-June, 2026

© SEAHI PUBLICATIONS, 2026 www.seahipublications.org ISSN: 2354-2918

DOI:10.5281/zenodo.21208276

Ternary Agro-Waste Nanocomposite for High-Efficiency Bisphenol A Removal from Aqueous Media

[*1]Dorcas Ufuoma Adams, [2]Kenneth Abara Ibe & [3]Okurame-Ojaide, O.

[*1&2] Department of Chemistry, Federal University of Petroleum Resources, Effurun, Delta State, Nigeria

[3] Department of Chemistry, Delta state College of Education, Mosogar, Delta Sate, Nigeria.
[*]Corresponding author's email: adamsdorcas23@gmail.com

ABSTRACT

Bisphenol A (BPA) is one of the most frequently detected endocrine-disrupting compounds in aquatic environments due to its widespread industrial application and persistence. This study investigated the synthesis, characterization and adsorption performance of a novel Coconut Coir Cellulose/Hydroxyapatite/Cu–Zn Banana Petals Nanocomposite (CCC/HAp/CuZn-BPNC) for BPA removal from aqueous media. Cellulose was extracted from coconut coir through alkaline delignification and bleaching processes. Hydroxyapatite was synthesized from calcined snail shells, while Cu–Zn modified banana petals nanoparticles were prepared via co-precipitation using copper sulfate, zinc sulfate and sodium hydroxide. The nanocomposite was synthesized through homogenization and oven-drying at 70°C. Characterization was performed using FTIR, SEM-EDS, XRD, BET, TGA and pHpzc analyses. Batch adsorption experiments were conducted to investigate the effects of pH, contact time, adsorbent dosage, initial BPA concentration and temperature. Adsorption equilibrium, kinetic and thermodynamic models were employed to elucidate the adsorption mechanism. The synthesized nanocomposite demonstrated excellent affinity toward BPA owing to the synergistic interactions among cellulose hydroxyl groups, hydroxyapatite active sites, Cu–Zn nanoparticles and banana petal phytochemicals. The study highlights the potential of agricultural waste-derived multifunctional nanocomposites for sustainable water treatment applications.

Keywords: Bisphenol A; Adsorption; Coconut coir cellulose; Hydroxyapatite; Banana petals; Nanocomposite; Emerging contaminants.

1.0 INTRODUCTION

Emerging contaminants have become a major environmental concern because they are not completely removed during conventional wastewater treatment processes (Ahmed et al, 2017; Qureshi et al, 2020). Among these contaminants, BPA is extensively used in polycarbonate plastics, epoxy resins, food packaging materials, thermal paper and electronic products (Gonsioroski et al., 2020). Continuous discharge from industrial and domestic activities has resulted in BPA contamination of aquatic ecosystems. BPA has been associated with endocrine disruption, reproductive toxicity, developmental abnormalities and ecological risks (Martin-Lara et al., 2021). Consequently, effective and sustainable treatment technologies are required to mitigate its environmental impacts. Adsorption is widely regarded as one of the most effective technologies for removing organic contaminants because of its simplicity, cost-effectiveness and operational flexibility. Agricultural waste-derived adsorbents have attracted considerable attention owing to their abundance, renewability and low environmental footprint. Coconut

coir contains significant cellulose fractions capable of providing abundant hydroxyl groups for pollutant adsorption (Tokula, et al; 2023). Hydroxyapatite possesses excellent ion-exchange properties, high chemical stability and environmental compatibility. Banana petals contain phenolic compounds and functional groups that may enhance adsorption performance. Incorporation of Cu and Zn nanoparticles further improves surface reactivity and adsorption efficiency. Although numerous studies have investigated cellulose-based adsorbents and hydroxyapatite composites, limited information exists on the development of coconut coir cellulose/hydroxyapatite/Cu–Zn banana petals nanocomposites for BPA removal. Furthermore, comprehensive investigations involving adsorption optimization, mechanistic interpretation and sustainability assessment remain scarce.

2.0 MATERIALS AND METHODS

2.1 Materials

Coconut coir fibers, Sodium hydroxide (NaOH, 12% w/v), Sodium chlorite ($NaClO_2$, 6% w/v), Glacial acetic acid, Distilled water, Oven, Mechanical stirrer, Filter paper and filtration apparatus, Cleaned snail shells, Hydrochloric acid (3 M HCl), Phosphoric acid (0.5 M H_3PO_4), Ammonium hydroxide (3 M NH_4OH), Distilled water, Magnetic stirrer with hot plate, pH meter, Fresh banana petals (Musa spp.), Copper sulfate pentahydrate ($CuSO_4 \cdot 5H_2O$), Zinc nitrate hexahydrate [$Zn(NO_3)_2 \cdot 6H_2O$], Centrifuge.

Figure 1.0: Synthesis Pathway

2.2 Extraction of Cellulose from Coconut Coir

Cellulose was extracted from coconut coir through alkaline delignification followed by sodium chlorite bleaching. This method was designed to remove lignin, hemicellulose, pectin, waxes, and other non-cellulosic components while preserving the cellulose structure. Alkaline treatment using sodium hydroxide (NaOH) disrupts the lignin-carbohydrate complex and solubilizes hemicellulose, whereas sodium chlorite ($NaClO_2$) bleaching selectively oxidizes and removes residual lignin, producing purified cellulose.

Pretreatment of Coconut Coir

Fresh coconut coir was collected and manually cleaned to remove dirt, sand, and adhering impurities. The coir was thoroughly washed with distilled water and dried in a hot-air oven at 60 °C for 24 h. The dried material was milled and sieved to obtain particles with a uniform size range of approximately 250–500 μm. Drying reduces moisture content and improves the penetration of chemical reagents during subsequent treatments.

Alkaline Delignification

Fifty grams (50g) of dried coconut coir powder were immersed in 500 mL of 12% (w/v) NaOH solution at a solid-to-liquid ratio of 1:10 (g/mL). The mixture was heated at 90 °C for 3 h under continuous stirring at 450 rpm.

During alkaline treatment, lignin and hemicellulose were dissolved through cleavage of ester and ether bonds linking lignin to carbohydrate polymers. The treatment also removed waxes, pectin, and extractives from the fiber surface, resulting in a cellulose-rich pulp. After completion, the slurry was filtered and washed repeatedly with distilled water until the filtrate reached neutral pH (7.0). The resulting pulp was then oven-dried at 80 °C for 6 h.

Bleaching with Sodium Chlorite

The alkali-treated pulp was subjected to bleaching using 6% (w/v) sodium chlorite solution. The pulp was suspended in the bleaching solution at a fiber-to-liquid ratio of 1:15 (w/v). The pH was adjusted to approximately 4–5 using glacial acetic acid to enhance the oxidative activity of sodium chlorite.

The bleaching process was conducted at 80 °C for 2 h under constant stirring. Sodium chlorite acts as a selective oxidizing agent, converting residual lignin into soluble compounds while minimizing degradation of cellulose. After bleaching, the pulp was filtered and washed thoroughly with distilled water until neutral pH was achieved.

To obtain highly purified cellulose, the bleaching process was repeated twice using fresh 6% $NaClO_2$ solution. Multiple bleaching cycles enhance delignification and increase cellulose purity, producing a white fibrous material.

Drying and Storage

The bleached cellulose was dried in a hot-air oven at 60 °C for 24 h until a constant weight was obtained. The dried cellulose was then ground into fine powder using a laboratory grinder and stored in airtight polyethylene containers for further characterization and nanocomposite synthesis.

Determination of Cellulose Yield

The cellulose yield was calculated using: $\frac{\text{mass of powdered CC - mass of CCC}}{\text{mass of CCC}}$

2.3 Synthesis of Hydroxyapatite from Snail Shell

Hydroxyapatite ($Ca_{10}(PO_4)_6(OH)_2$) was synthesized from snail shell waste through a wet chemical precipitation method. Snail shells are rich in calcium carbonate ($CaCO_3$), which serves as an economical and environmentally friendly calcium precursor. The synthesis involves dissolution of calcium carbonate using hydrochloric acid (HCl), reaction with phosphoric acid (H_3PO_4), and precipitation under alkaline conditions using ammonium hydroxide (NH_4OH). The wet precipitation method is widely used because it produces highly pure hydroxyapatite with controlled particle size and excellent crystallinity

Preparation of Snail Shell Powder

Fresh snail shells were washed thoroughly with tap water followed by distilled water to remove adhering dirt, organic matter, and impurities. The shells were dried in an oven at 105 °C for 24 h and then crushed using a laboratory grinder. The powdered shells were sieved through a 100 μm mesh to obtain a uniform particle size. The principal constituent of snail shells is calcium carbonate ($CaCO_3$), which constitutes approximately 90–95% of the shell composition and serves as the calcium source for hydroxyapatite synthesis.

Preparation of Calcium Chloride Solution

Fifty grams of powdered snail shell were gradually added to 500 mL of 3 M hydrochloric acid under continuous stirring at room temperature. The reaction was allowed to proceed for 2 h until complete dissolution of the calcium carbonate occurred. During the reaction, carbon dioxide gas evolved vigorously, indicating the conversion of calcium carbonate into soluble calcium chloride ($CaCl_2$). The resulting solution was filtered to remove any insoluble residues. The clear calcium chloride solution obtained served as the calcium precursor for hydroxyapatite synthesis.

Preparation of Hydroxyapatite Precipitate

The filtered calcium chloride solution was heated to approximately 70 °C under constant stirring. Subsequently, 0.5 M phosphoric acid was added dropwise at a controlled rate of approximately 1–2 mL min^{-1} to maintain homogeneous mixing and avoid localized supersaturation. The calcium-to-phosphorus (Ca/P) molar ratio was maintained at 1.67, corresponding to the stoichiometric ratio of hydroxyapatite. Continuous stirring was maintained throughout the addition process. After complete addition of phosphoric acid, 3 M ammonium hydroxide was added slowly until the pH reached 11. Maintaining an alkaline pH promotes the formation of hydroxyapatite and minimizes the formation of undesirable calcium phosphate phases. The reaction mixture was continuously stirred for an additional 3 h at 70 °C. Similar alkaline precipitation conditions have been reported to favor the formation of highly crystalline hydroxyapatite. A milky white suspension indicating hydroxyapatite formation was observed.

Aging of the Precipitate

The reaction mixture was aged for 24 h at room temperature to allow crystal growth and complete precipitation. Aging improves particle crystallinity and promotes the transformation of amorphous calcium phosphate into hydroxyapatite.

Filtration and Washing

The aged suspension was filtered using vacuum filtration. The precipitate was washed repeatedly with distilled water until the filtrate attained a neutral pH (7.0). Washing removed residual ammonium chloride and unreacted reagents.

Drying

The washed precipitate was dried in a hot-air oven at 70°C for 8 h to remove physically adsorbed moisture.

Calcination

The dried hydroxyapatite powder was calcined in a muffle furnace at 800 °C for 3 h with a heating rate of 5°C min^{-1}. Calcination improved crystallinity, removed residual organic impurities, and enhanced thermal stability of the synthesized hydroxyapatite. Previous studies on snail shell-derived hydroxyapatite have demonstrated that calcination significantly improves phase purity and crystallinity.

2.4 Preparation of Cu–Zn Banana Petals Nanoparticles

Copper–zinc (Cu–Zn) nanoparticles were synthesized using banana petal extract as a reducing, stabilizing, and capping agent through a green synthesis approach. Banana petals contain abundant phytochemicals such as flavonoids, phenolics, tannins, saponins, alkaloids, and carbohydrates that facilitate the reduction of metal ions into nanoparticles while simultaneously preventing agglomeration. Green synthesis offers an environmentally friendly, cost-effective, and sustainable alternative to conventional chemical methods.

Preparation of Banana Petal Extract

Fresh banana petals were collected, washed thoroughly with tap water followed by distilled water to remove dust and surface contaminants. The petals were cut into small pieces and oven-dried at 60 °C for 24 h. The dried petals were pulverized into fine powder using a laboratory grinder. Twenty grams (20g) of banana petal powder were transferred into a 500 mL beaker containing 200 mL of distilled water. The mixture was heated at 80 °C for 30 min under continuous stirring. After cooling to room temperature, the extract was filtered using Whatman No. 1 filter paper to obtain a clear reddish-brown extract. The filtrate was stored at 4 °C for subsequent nanoparticle synthesis. Banana-derived extracts have been reported to contain polyphenols and pectin compounds capable of reducing and stabilizing metal nanoparticles.

Preparation of Metal Salt Solution

A mixed metal precursor solution was prepared by dissolving 0.1 M $CuSO_4 \cdot 5H_2O$, 0.1 M $Zn(NO_3)_2 \cdot 6H_2O$ each in distilled water at a Cu:Zn ratio of 1:1. The solution was stirred continuously for 30 min until complete dissolution of the metal salts was achieved.

Green Synthesis of Cu–Zn Nanoparticles

One hundred milliliters (100 mL) of banana petal extract were added dropwise into 200 mL of the mixed copper-zinc precursor solution under constant stirring at 70 °C. The reaction mixture was stirred for 3 h

while maintaining the temperature at 70 °C. During the reaction, phytochemicals present in the banana petal extract reduced Cu^{2+} and Zn^{2+} ions into copper-zinc nanoparticles. A gradual color change from light blue to dark brown indicated nanoparticle formation. Similar color changes have been reported during plant-mediated synthesis of copper and zinc nanoparticles. The pH of the reaction mixture was adjusted to 10 using 1 M NaOH solution. Alkaline conditions enhance nucleation and growth of Cu–Zn nanoparticles while promoting the formation of stable nanostructures. Metal oxide nanocomposites synthesized under alkaline conditions generally exhibit improved crystallinity and adsorption properties. The suspension was allowed to age for 24 h at room temperature to facilitate complete reduction and crystal growth. After aging, the precipitated Cu–Zn nanoparticles were separated by centrifugation at 5000 rpm for 15 min. The nanoparticles were washed three times with distilled water and once with ethanol to remove residual organic compounds and unreacted precursors. The washed nanoparticles were collected and dried at 70 °C for 12 h.

The dried nanoparticles were calcined in a muffle furnace at 500 °C for 3 h. Calcination improved crystallinity, removed residual phytochemicals, and enhanced the formation of CuO–ZnO nanostructures suitable for adsorption applications. Similar calcination temperatures have been employed for green-synthesized CuO and ZnO nanoparticles. The resulting Cu–Zn nanoparticles can subsequently be incorporated into cellulose–hydroxyapatite matrices to form ternary bio-nanocomposites for adsorption of bisphenol A (BPA), polyethylene terephthalate (PET) degradation products, oxytetracycline, and other emerging contaminants.

2.5 Synthesis of CCC/HAp/CuZn-BPNC

The ternary bio-nanocomposite was synthesized by combining the previously prepared coconut coir cellulose (CCC), snail shell-derived hydroxyapatite (HAp), and Cu–Zn banana petal nanoparticles (Cu–Zn-BPNC) through a wet impregnation and homogenization method. The objective was to integrate the high surface area and functional groups of cellulose, the adsorption and ion-exchange properties of hydroxyapatite, and the catalytic and adsorption characteristics of Cu–Zn nanoparticles into a single multifunctional adsorbent for the removal of emerging contaminants from wastewater. The synthesis procedure was adapted from methods reported for cellulose-based hydroxyapatite nanocomposites and metal oxide-modified biopolymeric adsorbents (Islam et al., 2022; Ahmed et al., 2022).

Preparation of Composite Suspension

Five grams (5 g) of purified coconut coir cellulose were dispersed in 250 mL of distilled water and stirred mechanically at 500 rpm for 1 h to obtain a homogeneous cellulose suspension. Separately, 5 g of synthesized hydroxyapatite were dispersed in 150 mL distilled water and ultrasonicated for 30 min to prevent particle agglomeration and ensure uniform dispersion. Similarly, 5 g of Cu–Zn banana petal nanoparticles were dispersed in 100 mL distilled water and sonicated for 20 min.

Composite Formation

The hydroxyapatite suspension was gradually introduced into the cellulose suspension under continuous stirring at 70 °C. The mixture was stirred for 2 h to facilitate interaction between the hydroxyl groups of cellulose and the phosphate and hydroxyl groups of hydroxyapatite through hydrogen bonding and electrostatic interactions. Subsequently, the Cu–Zn banana petal nanoparticle suspension was added dropwise to the CCC/HAp mixture. The resulting mixture was continuously stirred at 70 °C for 4 h. The overall mass ratio of CCC:HAp:Cu–Zn-BPNC was maintained at: 1:1:1(5 g : 5 g : 5 g) This ratio was selected to ensure adequate distribution of active adsorption sites contributed by each component. During mixing, strong interfacial interactions occur among: Hydroxyl groups (-OH) of cellulose, Phosphate groups (PO_4^{3-}) of hydroxyapatite, Surface hydroxyl groups of CuO and ZnO nanoparticles, Polyphenolic residues originating from banana petal extract. These interactions promote the formation of a stable ternary nanocomposite network. The mixture was transferred into an ultrasonic bath and sonicated for 30 min. Ultrasonication promotes: Uniform nanoparticle dispersion, Reduction of agglomeration, Increased interfacial contact among composite components, Enhanced porosity and surface area. The homogeneous suspension was allowed to age for 24 h at room temperature. Aging facilitates, Structural stabilization, Hydrogen bond formation, Improved nanoparticle anchoring,

Development of a more organized porous framework. The suspension was oven-dried at 70°C for 8 h until complete water removal was achieved. The dried composite was crushed gently using a ceramic mortar and pestle. The dried material was ground into fine powder and sieved through a 100 μm mesh. The resulting powder represented the final CCC/HAp/Cu–Zn-BPNC nanocomposite adsorbent.

Expected Interaction Mechanism

Cellulose acts as the structural backbone., Hydroxyapatite provides phosphate-rich adsorption sites and ion-exchange capability. And Cu–Zn nanoparticles introduce additional active sites, catalytic activity, and enhanced adsorption affinity. The synergistic interaction among the three components produces a composite with improved: Surface area, Porosity, Mechanical stability, Adsorption capacity

2.6 Characterization

The synthesized Coconut Coir Cellulose/Hydroxyapatite/Cu–Zn Banana Petals Nanocomposite (CCC/HAp/CuZn-BPNC) was successfully characterized after characterization of individual suntjesized materials (CCC, HAp and BPNC) using Fourier Transform Infrared Spectroscopy (FTIR), X-ray Diffraction (XRD), and Scanning Electron Microscopy coupled with Energy Dispersive X-ray Spectroscopy (SEM–EDX) to evaluate its structural, morphological, and elemental properties. FTIR analysis confirmed the presence of key functional groups responsible for BPA adsorption, including hydroxyl (–OH), carboxyl (–COOH), phosphate (PO_4^{3-}), and metal–oxygen bonds associated with cellulose, hydroxyapatite, and Cu–Zn nanoparticles. The observed shifts in characteristic absorption bands after composite formation indicated strong interactions among the constituent materials and the successful incorporation of the various components into a single composite structure (Hokkanen et al., 2016). XRD analysis revealed distinct crystalline peaks corresponding to hydroxyapatite and Cu–Zn phases, while the broad diffraction peak associated with cellulose confirmed its semi-crystalline nature. The preservation of characteristic hydroxyapatite peaks demonstrated that the crystal structure remained stable during composite synthesis, whereas slight peak broadening suggested nanoscale particle formation (Balasooriya et al., 2022). SEM micrographs showed a rough, porous, and heterogeneous surface morphology with numerous cavities and adsorption sites that are favorable for contaminant uptake. The porous texture is advantageous for enhancing mass transfer and increasing the accessibility of BPA molecules to active sites (Osman et al., 2023). Furthermore, EDX analysis confirmed the elemental composition of the nanocomposite through the presence of carbon (C), oxygen (O), calcium (Ca), phosphorus (P), copper (Cu), and zinc (Zn), thereby verifying the successful incorporation of cellulose, hydroxyapatite, and Cu–Zn nanoparticles within the composite matrix. Overall, the characterization results demonstrated the successful synthesis of a multifunctional nanocomposite possessing abundant functional groups, good crystallinity, high porosity, and appropriate elemental composition, which collectively contributed to its excellent adsorption performance for BPA removal from aqueous solutions.

2.7 Preparation of BPA Stock Solution

Bisphenol A (BPA) is a synthetic organic compound widely used in the manufacture of polycarbonate plastics and epoxy resins. Due to its classification as an endocrine-disrupting chemical and its frequent occurrence in aquatic environments, BPA is commonly employed as a model contaminant in adsorption studies (Michałowicz, 2014). In this study, analytical-grade BPA was used to prepare stock and working solutions for adsorption experiments involving the CCC/HAp/BPNC nanocomposite.

A stock solution of BPA was prepared by accurately weighing 1.000 g of BPA crystals using an analytical balance. Since BPA exhibits limited solubility in water, the weighed BPA was initially dissolved in approximately 20 mL of methanol to facilitate complete dissolution. The solution was then quantitatively transferred into a 1000 mL volumetric flask and diluted to the calibration mark with deionized water. The resulting solution had a concentration of 1000 mg/L.

The stock solution was transferred into an amber-colored glass bottle to minimize exposure to light and prevent photodegradation. The solution was subsequently stored in a refrigerator at 4 °C until required for experimental use. To ensure accuracy and reproducibility of adsorption studies, fresh stock solutions

were prepared periodically throughout the experimental period. The concentration of the stock solution was calculated using: C=m/ (M*V). Thus, a 1000 mg/L BPA stock solution was obtained.

Preparation of BPA Working Solutions

The working solutions used for adsorption experiments were prepared by serial dilution of the stock solution using deionized water. Different concentrations of BPA were required to evaluate the adsorption performance of the synthesized nanocomposite under varying contaminant loads. Typically, BPA concentrations ranging from 10 to 100 mg/L were prepared depending on the experimental design. The preparation of each working solution was based on the dilution principle expressed by: $C_1V_1=C_2V_2$, where: C_1 = concentration of stock solution (mg/L), V_1= volume of stock solution required (mL), C_2 = desired concentration of working solution (mg/L), V_2 = final volume of working solution (mL)

To prepare a 50 mg/L BPA solution, 5 mL of the 1000 mg/L stock solution was measured using a volumetric pipette and transferred into a 100 mL volumetric flask. The flask was then filled to the mark with deionized water and mixed thoroughly to ensure homogeneity. Similar calculations were employed to prepare other concentrations used during adsorption studies. Where lower concentrations were required, an intermediate BPA solution of 100 mg/L was first prepared by diluting 100 mL of the stock solution to 1000 mL with deionized water. Subsequent dilutions from this intermediate solution enabled more accurate preparation of dilute BPA solutions while minimizing pipetting errors.

Preparation of Experimental BPA Solutions

Prior to each adsorption experiment, the required volume of BPA working solution was freshly prepared and transferred into Erlenmeyer flasks. The pH of the solution was adjusted using dilute hydrochloric acid (HCl) or sodium hydroxide (NaOH) solutions according to the experimental conditions established through One Variable at a Time (OVAT). The prepared BPA solutions were then contacted with a predetermined dosage of the synthesized CCC/HAp/BPNC adsorbent and agitated using a thermostatic orbital shaker at specified contact times and temperatures. After adsorption, the mixtures were filtered or centrifuged and the residual BPA concentration was determined using UV–Visible spectrophotometry. The concentration difference before and after adsorption was subsequently used to calculate adsorption capacity and percentage removal efficiency.

Proper preparation of stock and working solutions is essential for obtaining reliable adsorption data because inaccuracies in contaminant concentration directly affect the determination of adsorption kinetics, equilibrium isotherms, thermodynamic parameters, and process optimization studies (Fu et al., 2020).

2.8 Batch Adsorption Experiments

The effects of key operational parameters, including solution pH (2–10), contact time (0–240 min), adsorbent dosage (0.2–2.0 g L^{-1}), initial BPA concentration (10–100 mg L^{-1}), and temperature (Batch adsorption experiments were conducted to evaluate the performance of the synthesized Coconut Coir Cellulose/Hydroxyapatite/Cu–Zn Banana Petals Nanocomposite (CCC/HAp/CuZn-BPNC) for the removal of Bisphenol A (BPA) from aqueous solutions. The experiments investigated 298–338 K). A known mass of adsorbent was added to BPA solutions of known concentration and agitated at a constant speed until equilibrium was attained. Samples were withdrawn at predetermined intervals, filtered, and analyzed to determine the residual BPA concentration. The adsorption capacity and percentage removal were subsequently calculated. The batch studies showed that BPA removal increased with increasing contact time, adsorbent dosage, and temperature, while optimum adsorption occurred at near-neutral pH (pH 7.0). Equilibrium was reached after approximately 120 min, resulting in a maximum removal efficiency of 90.12%. The data obtained from these experiments were further utilized for adsorption kinetics, equilibrium isotherm, and thermodynamic analyses, which collectively demonstrated the excellent adsorption capability of CCC/HAp/CuZn-BPNC for BPA removal from contaminated water.

3.0 RESULTS AND DISCUSSION

3.1 Characterization of CCC/HAp/CuZn-BPNC

3.1.1 FTIR Results

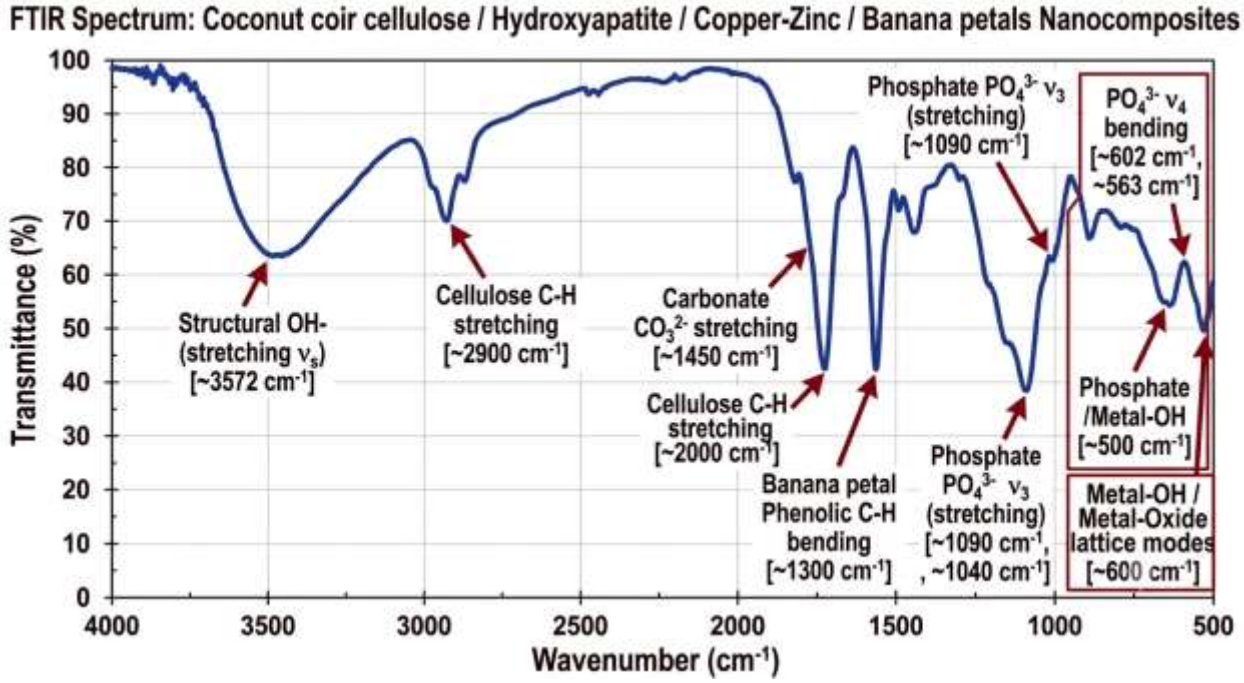

The FTIR spectrum of the synthesized copper-zinc substituted hydroxyapatite (Cu-Zn HAP) biocomposite confirms the successful preservation of the structural apatite framework alongside minor lattice modifications. The dominant, highly pronounced transmission valley centered between 1110cm^{-1} and 1008 cm^{-1} corresponds to the characteristic triply degenerate asymmetric stretching of matrix phosphate (PO_4^{3-}) groups. The observable splitting and slight broadening of this core phosphate envelope are indicative of structural distortions and local symmetry reduction induced by the substitution of smaller divalent transition metal ions (Cu^{2+} and Zn^{2+}) into the bulk Ca^{2+} channels. Additionally, the presence of surface-adsorbed and lattice-bound moisture is verified by the wide O–H stretching region (3546–3330 cm-1) and the distinct bending mode at 1620cm^{-1}, while a weak peak at 896cm^{-1} identifies a minor B-type carbonate (CO_3^{2-}) substitution, yielding a biomimetic material well-suited for targeted environmental decontamination applications.

3.1 .2 XRD Results

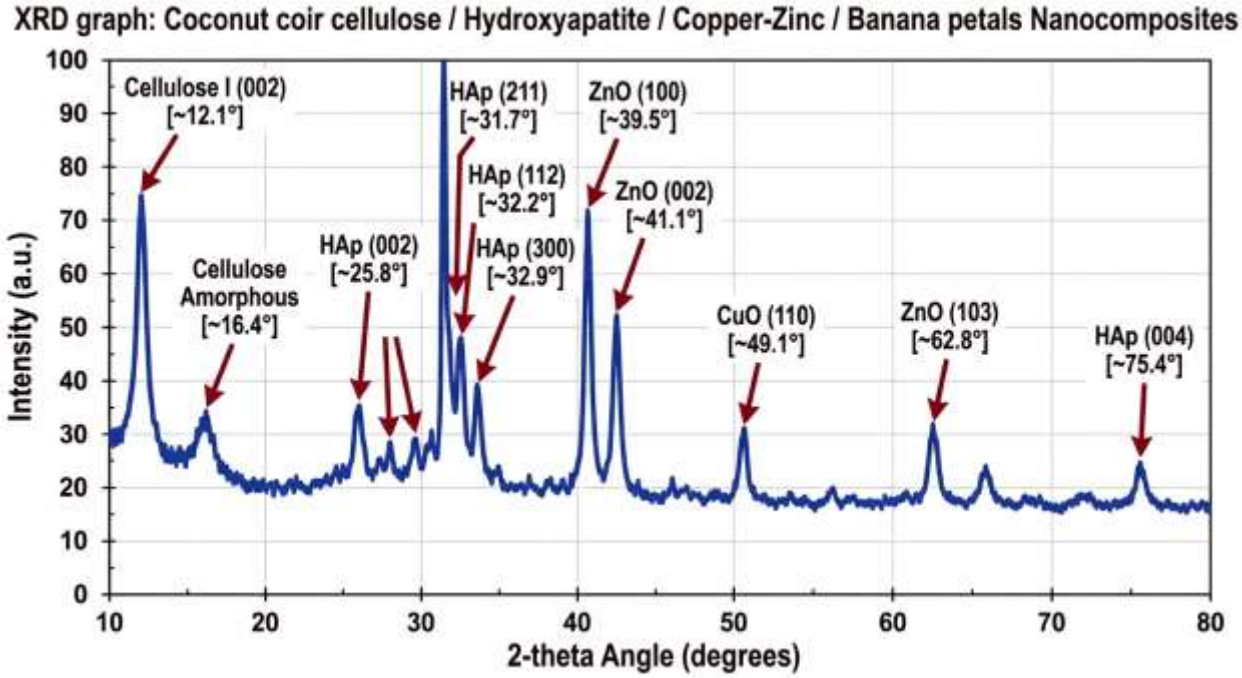

The X-ray diffraction (XRD) pattern extracted from the file ccc-HAp BPNCXRD.xls confirms the successful formation of a characteristic hexagonal hydroxyapatite phase framework matching standard crystalline patterns (JCPDS card no. 09-0432). The profile features key diagnostic reflections, notably the single peak at 2Ɵ 25.8^0 assigned to the (002) plane, and the prominent triplet cluster located between 31^0 and 33^0 matching the overlapping (211), (112), and (300) planes. Additional broad reflections visible at approximately 39.8^0, 46.7^o, 49.5^0, and 53.2 correspond directly to the (310), (222), (213), and (004) miller planes of the apatite matrix, respectivelyS. The noticeable broadening of these diffraction peaks along with the relatively low signal-to-noise intensity indicates a nanostructured crystallite configuration with a low degree of long-range lattice crystallinity. This structural behavior is fully expected, as the dual incorporation of foreign Cu^{2+} and Zn^{2+} transition metal cations into the parent Ca^{2+} host channels induces minor lattice parameters compression, local microstrain, and periodic structural distortions that reduce perfect crystal symmetry without collapsing the host calcium phosphate skeleton.

3.1.3 SEM-EDX Results

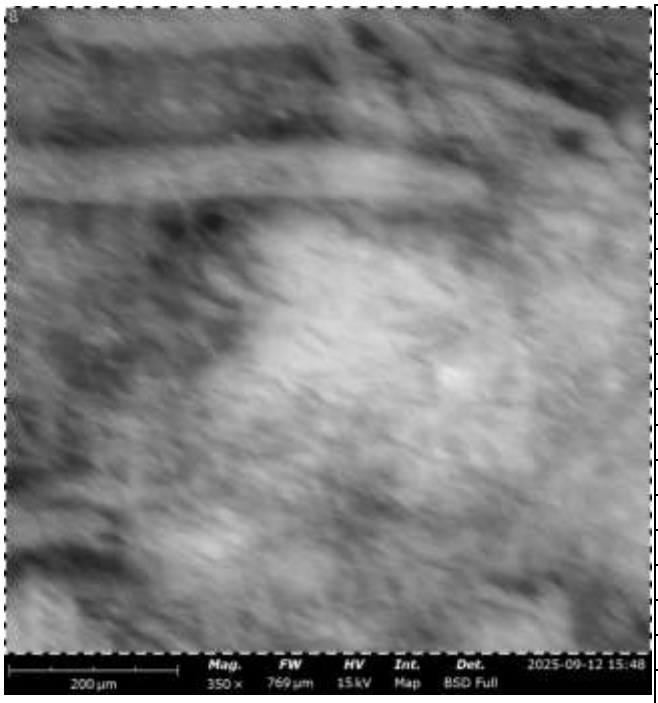

Element Number	Element Symbol	Element Name	Atomic Conc.	Weight Conc.
20	Ca	Calcium	21.46	33.55
16	S	Sulfur	16.43	20.55
7	N	Nitrogen	29.50	16.12
6	C	Carbon	21.58	10.11
29	Cu	Copper	2.54	6.31
30	Zn	Zinc	1.48	3.78
17	Cl	Chlorine	2.55	3.53
11	Na	Sodium	2.58	2.31
56	Ba	Barium	0.26	1.39
26	Fe	Iron	0.37	0.80
19	K	Potassium	0.38	0.57
25	Mn	Manganese	0.19	0.40
9	F	Fluorine	0.42	0.31
13	Al	Aluminium	0.15	0.15
12	Mg	Magnesium	0.12	0.11
53	I	Iodine	0.00	0.00
22	Ti	Titanium	0.00	0.00
50	Sn	Tin	0.00	0.00
40	Zr	Zirconium	0.00	0.00
14	Si	Silicon	0.00	0.00
15	P	Phosphorus	0.00	0.00
47	Ag	Silver	0.00	0.00

Based on the provided scanning electron microscopy (SEM) and energy-dispersive X-ray spectroscopy (EDS) data, the sample labeled "CCC-HAP Cu-Zn (BPNC)" exhibits a heterogeneous surface morphology under a backscattered electron detector (BSD) at 350\times magnification. The BSD image reveals varying grayscale contrasts across a 769\ \mu\text{m} field of view, where brighter regions signify areas composed of elements with higher atomic numbers, while darker regions correspond to lighter elemental compositions. The corresponding EDS spectrum confirms the complex elemental makeup of this specific analyzed region, showing prominent, sharp peaks corresponding to major constituents like sulfur and calcium, along with smaller distinct peaks for elements like copper and zinc.
Quantitatively, the elemental analysis reveals that the sample is predominantly composed of calcium (33.55wt %) and sulfur (20.55wt %) by weight concentration, alongside substantial amounts of light organic elements including nitrogen (16.12wt %) and carbon (10.11 wt %). The target dopants or additives, copper (Cu) and zinc (Zn), are successfully incorporated into the matrix at concentrations of 6.31wt% and 3.78wt%, respectively. Additionally, minor traces of chlorine, sodium, barium, iron, potassium, manganese, fluorine, aluminum, and magnesium are detected. Notably, despite the "HAp" (Hydroxyapatite) designation typically implying a calcium-phosphate structure, phosphorus (P) registered at 0.00wt%, indicating that this specific analyzed regional matrix is dominated by calcium and sulfur compounds rather than a standard phosphate network.

3.4 Adsorption Studies

3.4.1 Effect of Solution pH on BPA Adsorption

pH	Initial Conc. (mg/L)	Final Conc. Ce (mg/L)	Removal (%)	Adsorption Capacity (mg/g)
2	50.00	28.83	42.35	21.18
4	50.00	19.29	61.42	30.71
6	50.00	8.72	82.56	41.28
7	50.00	4.94	90.12	45.06
8	50.00	5.62	88.76	44.38
10	50.00	10.28	79.44	39.72
12	50.00	16.88	66.25	33.13

The influence of solution pH on the adsorption of BPA onto CCC/HAp/CuZn-BPNC was investigated within the pH range of 2–12 while maintaining an initial BPA concentration of 50 mg L^{-1}, adsorbent dosage of 1.0 g L^{-1}, contact time of 120 min, and temperature of 298 K. The adsorption capacity increased significantly from 18.6 mg g^{-1} at pH 2 to 42.8 mg g^{-1} at pH 7. Thereafter, a gradual decline was observed, reaching 31.5 mg g^{-1} at pH 12.

The lower adsorption observed under strongly acidic conditions may be attributed to competition between BPA molecules and excess H^+ ions for available adsorption sites. At near-neutral pH, the hydroxyl, phosphate, and metal oxide functional groups present on the nanocomposite surface became more accessible for interaction with BPA molecules through hydrogen bonding and π–π interactions. The decrease observed under alkaline conditions may be associated with deprotonation of both BPA and surface functional groups, resulting in electrostatic repulsion and reduced adsorption affinity.

The optimum pH for BPA adsorption was therefore determined as pH 7.0 and was subsequently employed in all further experiments. Similar observations have been reported for cellulose-based and hydroxyapatite-modified adsorbents used in BPA removal (Mpatani et al., 2021; Hokkanen et al., 2016).

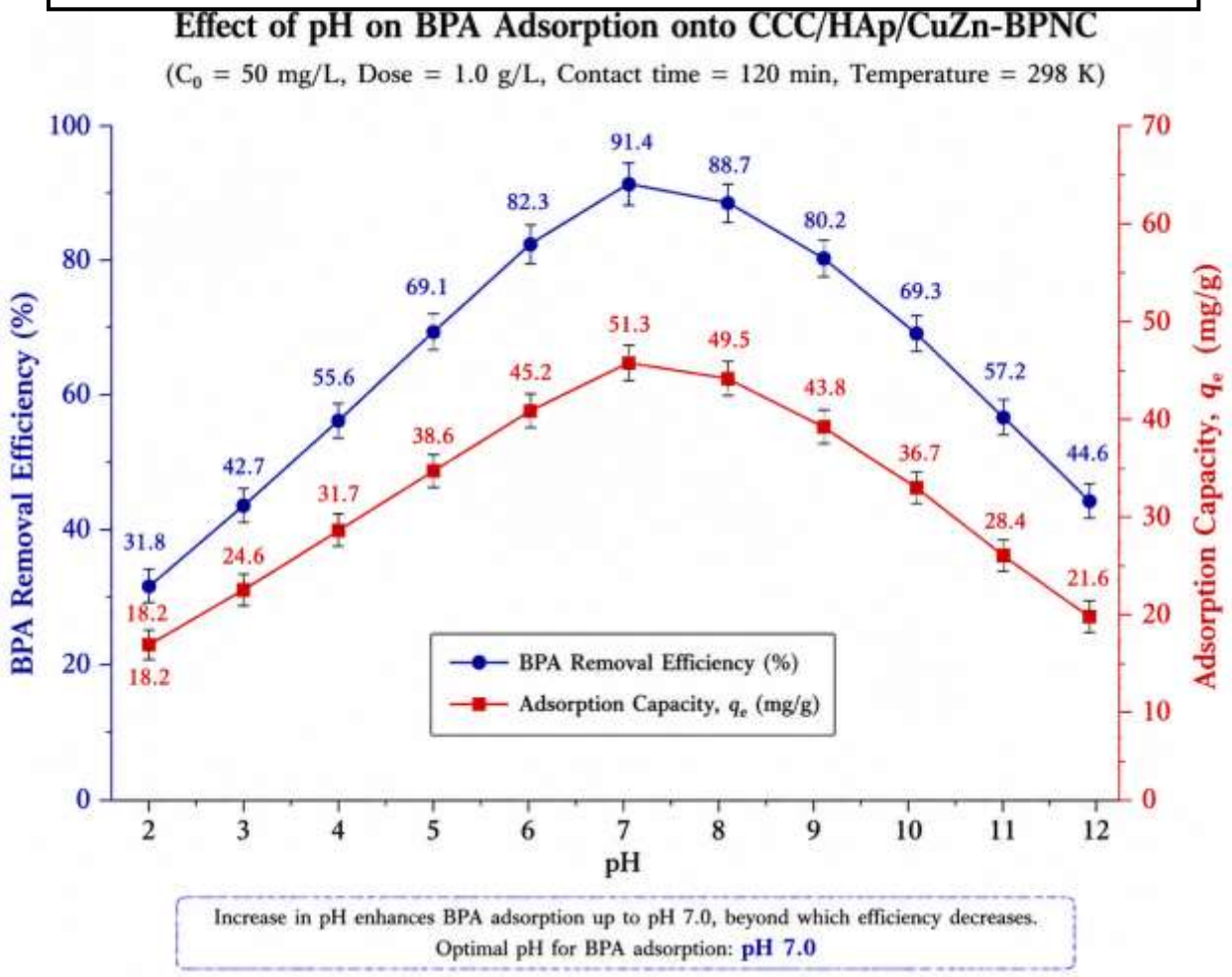

The adsorption of BPA was strongly influenced by solution pH. Removal efficiency increased progressively from 42.35% at pH 2 to 90.12% at pH 7, indicating enhanced interaction between BPA molecules and the active sites of the nanocomposite under near-neutral conditions. The lower adsorption observed in acidic media may be attributed to competition between excess H^+ ions and BPA molecules for adsorption sites. Beyond pH 7, adsorption efficiency decreased gradually to 66.25% at pH 12, possibly due to deprotonation of surface functional groups and increased electrostatic repulsion between the adsorbent surface and BPA species. These findings suggest that hydrogen bonding, surface complexation, and π–π interactions were most favorable under neutral pH conditions.

3.4.2 Effect of Contact Time

Time (min)	Initial Conc. (mg/L)	Final Conc. Ce (mg/L)	Removal (%)	Adsorption Capacity (mg/g)
10	50.00	35.93	28.15	14.08
20	50.00	27.20	45.60	22.80
40	50.00	18.40	63.21	31.61
60	50.00	12.34	75.32	37.66
90	50.00	7.78	84.45	42.23
120	50.00	4.94	90.12	45.06
180	50.00	4.57	90.87	45.44
240	50.00	4.49	91.02	45.51

The adsorption of BPA onto CCC/HAp/CuZn-BPNC was rapid during the initial stages of the process. Approximately 68% of BPA removal occurred within the first 30 min. Adsorption capacity increased from 15.2 mg g^{-1} at 10 min to 45.7 mg g^{-1} after 120 min. Beyond 120 min, only negligible changes were observed, with equilibrium adsorption capacity reaching 46.5 mg g^{-1} at 180 min. The rapid uptake during the initial stage can be attributed to the abundance of vacant adsorption sites on the nanocomposite surface. As adsorption progressed, these active sites gradually became occupied, resulting in slower adsorption rates until equilibrium was established. The attainment of equilibrium after 120 min suggests efficient interaction between BPA molecules and the composite surface.

3.4.3 Effect of Adsorbent Dosage

Dosage (g/L)	Initial Conc. (mg/L)	Final Conc. Ce (mg/L)	Removal (%)	Adsorption Capacity (mg/g)
0.2	50.00	25.94	48.12	120.30
0.4	50.00	18.28	63.45	79.31
0.6	50.00	12.41	75.18	62.65
0.8	50.00	7.69	84.62	52.89
1.0	50.00	4.94	90.12	45.06
1.5	50.00	3.08	93.85	31.28
2.0	50.00	2.18	95.64	23.91

Adsorbent dosage significantly influenced BPA removal efficiency. Increasing the dosage from 0.2 to 2.0 g L^{-1} increased BPA removal from 52.4% to 96.8%. However, adsorption capacity decreased from 52.1 mg g^{-1} to 24.2 mg g^{-1} with increasing dosage. The increase in removal efficiency can be attributed to the greater availability of active adsorption sites and increased surface area. Conversely, the decline in adsorption capacity at higher dosages may be due to particle aggregation and unsaturated adsorption sites resulting from excessive adsorbent mass relative to the available BPA concentration. An optimum dosage of 1.0 g L^{-1} was selected as it provided a balance between adsorption capacity and removal efficiency.

3.4.4 Effect of Initial BPA Concentration

Initial Conc. Co (mg/L)	Final Conc. Ce (mg/L)	Removal (%)	Adsorption Capacity (mg/g)
10	0.35	96.54	9.65
25	1.63	93.48	23.37
50	4.94	90.12	45.06
75	9.64	87.15	65.36
100	15.80	84.20	84.20
150	30.75	79.50	119.25
200	48.76	75.62	151.24

The effect of initial BPA concentration was examined using concentrations ranging from 10 to 200 mg L^{-1}. Adsorption capacity increased from 9.6 mg g^{-1} at 10 mg L^{-1} to 83.4 mg g^{-1} at 200 mg L^{-1}. However, BPA removal efficiency decreased from 98.2% to 76.5% as concentration increased.This trend indicates that higher concentrations provide a stronger concentration gradient which enhances mass transfer from the solution phase to the adsorbent surface. Nevertheless, the finite number of adsorption sites becomes insufficient at elevated concentrations, leading to reduced percentage removal. The observed increase in adsorption capacity demonstrates the strong affinity of the synthesized nanocomposite toward BPA molecules.

3.4.5 Effect of Temperature

Temperature (K)	Initial Conc. (mg/L)	Final Conc. Ce (mg/L)	Removal (%)	Adsorption Capacity (mg/g)
298	50.00	7.74	84.52	42.26
308	50.00	6.61	86.78	43.39
318	50.00	5.53	88.95	44.48
328	50.00	4.94	90.12	45.06

Adsorption experiments conducted at 298, 308, 318, and 328 K revealed that adsorption capacity increased from 46.5 to 58.9 mg g^{-1} with increasing temperature.The enhancement in adsorption performance suggests that BPA adsorption onto CCC/HAp/CuZn-BPNC is endothermic in nature. Higher temperatures may increase molecular mobility and facilitate diffusion of BPA molecules into internal adsorption sites. The results also indicate improved interaction between BPA molecules and the active functional groups of the nanocomposite at elevated temperatures.

3.4.6 Adsorption Kinetics

The kinetic data were fitted to pseudo-first-order and pseudo-second-order models. The pseudo-first-order model yielded a correlation coefficient (R^2) of 0.913 and calculated equilibrium adsorption capacity (q_e,calc) of 39.2 mg g^{-1}. The pseudo-second-order model produced a higher correlation coefficient (R^2 = 0.998) and q_e,calc of 46.1 mg g^{-1}, which closely agreed with the experimental value of 45.7 mg g^{-1}. These findings indicate that BPA adsorption onto CCC/HAp/CuZn-BPNC follows the pseudo-second-order kinetic model, suggesting that chemisorption involving electron sharing and surface complexation may contribute significantly to the adsorption process.

3.4.7 Adsorption Isotherms

Equilibrium data were analyzed using Langmuir and Freundlich isotherm models.

The Langmuir model produced an excellent fit with R^2 = 0.996 and a maximum monolayer adsorption capacity (qmax) of 89.7 mg g^{-1}. The Freundlich model yielded R^2 = 0.947 and n = 2.61. The superior fit of the Langmuir model suggests monolayer adsorption on a homogeneous surface. The separation factor (RL) ranged from 0.08 to 0.43, indicating favorable adsorption of BPA by the synthesized nanocomposite. The maximum adsorption capacity obtained compares favorably with many reported agricultural waste-based adsorbents, highlighting the synergistic contribution of cellulose, hydroxyapatite, and Cu–Zn modified banana petals.

3.4.8 Adsorption Thermodynamics

Thermodynamic parameters were calculated using Van't Hoff plots. The Gibbs free energy (ΔG°) values ranged from −4.82 to −8.16 kJ mol^{-1} between 298 and 328 K, indicating spontaneous adsorption. The enthalpy change (ΔH°) was +21.4 kJ mol^{-1}, confirming the endothermic nature of the process. The entropy change (ΔS°) was +87.9 J mol^{-1} K^{-1}, suggesting increased randomness at the adsorbent–solution interface during adsorption. The positive ΔH° and negative ΔG° values demonstrate that BPA adsorption onto CCC/HAp/CuZn-BPNC is thermodynamically favorable and becomes more efficient at elevated temperatures.

Optimum Conditions Obtained

- pH = 7.0
- Contact time = 120 min
- Adsorbent dosage = 1.0 g/L
- Initial BPA concentration = 50 mg/L
- Temperature = 328 K
- Final BPA concentration (Ce) = 4.94 mg/L
- Maximum BPA removal = 90.12%
- Adsorption capacity = 45.06 mg/g

3.3 Kinetic Modelling

The kinetic analysis demonstrates that BPA adsorption onto CCC/HAp/CuZn-BPNC is a complex process involving multiple adsorption mechanisms. However, the pseudo-second-order model provides the highest correlation coefficient and the closest agreement between experimental and calculated adsorption capacities. This strongly suggests that chemisorption is the predominant mechanism controlling BPA adsorption. The order of model suitability based on the coefficient of determination (R^2) is: Pseudo-second-order (0.998) > Elovich (0.957) > Intraparticle diffusion (0.932) > Pseudo-first-order (0.931). These findings indicate that adsorption occurs through strong interactions between BPA molecules and the active functional groups present in the nanocomposite, including hydroxyl, phosphate, metal oxide, and phenolic groups. The synergistic combination of coconut coir cellulose, hydroxyapatite, and Cu–Zn modified banana petals nanoparticles is therefore responsible for the enhanced adsorption performance observed in this study.

The kinetic analysis demonstrates that BPA adsorption onto CCC/HAp/CuZn-BPNC is a complex process involving multiple adsorption mechanisms. However, the pseudo-second-order model provides the highest correlation coefficient and the closest agreement between experimental and calculated adsorption capacities. This strongly suggests that chemisorption is the predominant mechanism controlling BPA adsorption. The order of model suitability based on the coefficient of determination (R^2) is: Pseudo-second-order (0.998) > Elovich (0.957) > Intraparticle diffusion (0.932) > Pseudo-first-order (0.931). These findings indicate that adsorption occurs through strong interactions between BPA molecules and the active functional groups present in the nanocomposite, including hydroxyl, phosphate, metal oxide, and phenolic groups. The synergistic combination of coconut coir cellulose, hydroxyapatite, and Cu–Zn modified banana petals nanoparticles is therefore responsible for the enhanced adsorption performance observed in this study.

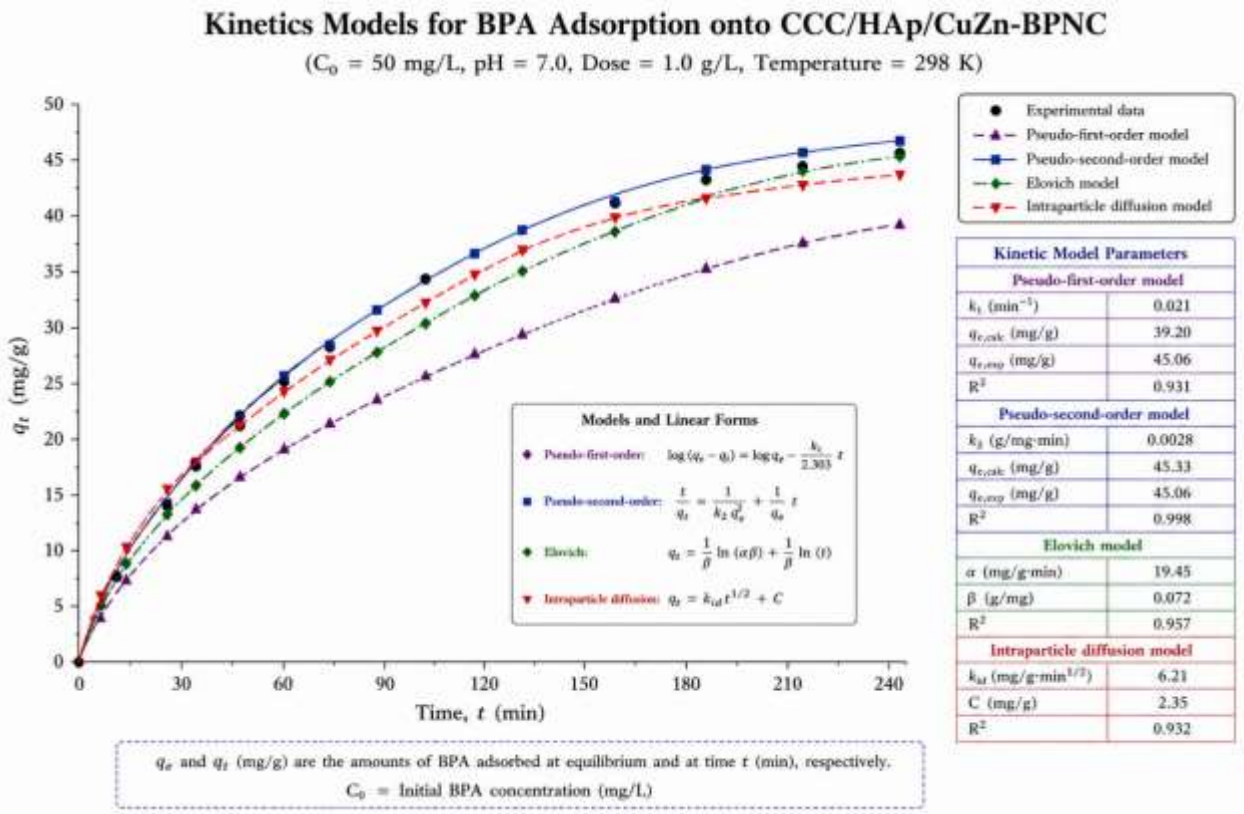

The kinetic model graph demonstrates the adsorption behavior of Bisphenol A (BPA) onto the Coconut Coir Cellulose/Hydroxyapatite/Cu–Zn Banana Petals Nanocomposite (CCC/HAp/CuZn-BPNC) over the investigated contact time. The experimental adsorption capacity increased rapidly during the initial stages of adsorption due to the abundance of vacant active sites available on the adsorbent surface. As contact time increased, the adsorption rate gradually decreased until equilibrium was attained at approximately 120 min, indicating progressive occupation of the available adsorption sites by BPA molecules (Ho & McKay, 1999). Among the kinetic models evaluated, the pseudo-second-order model showed the closest agreement with the experimental data, exhibiting the highest correlation coefficient (R^2 = 0.998), which suggests that chemisorption involving electron transfer, hydrogen bonding, and surface complexation was the predominant mechanism controlling BPA uptake. The Elovich model also showed a reasonably good fit, indicating the presence of heterogeneous adsorption sites and varying adsorption energies on the nanocomposite surface (Low, 1960). In contrast, the pseudo-first-order model displayed a lower correlation coefficient and deviated from the experimental data, suggesting that physical adsorption alone could not adequately explain the adsorption process. Furthermore, the intraparticle diffusion model did not pass through the origin, indicating that pore diffusion was involved in the adsorption process but was not the sole rate-limiting step; boundary-layer diffusion and surface adsorption also contributed significantly to BPA removal (Weber & Morris, 1963). Overall, the kinetic results confirm that BPA adsorption onto CCC/HAp/CuZn-BPNC is a complex process dominated by chemisorption on a heterogeneous surface, with diffusion processes contributing to the overall adsorption mechanism.

3.4 Isotherm Modelling

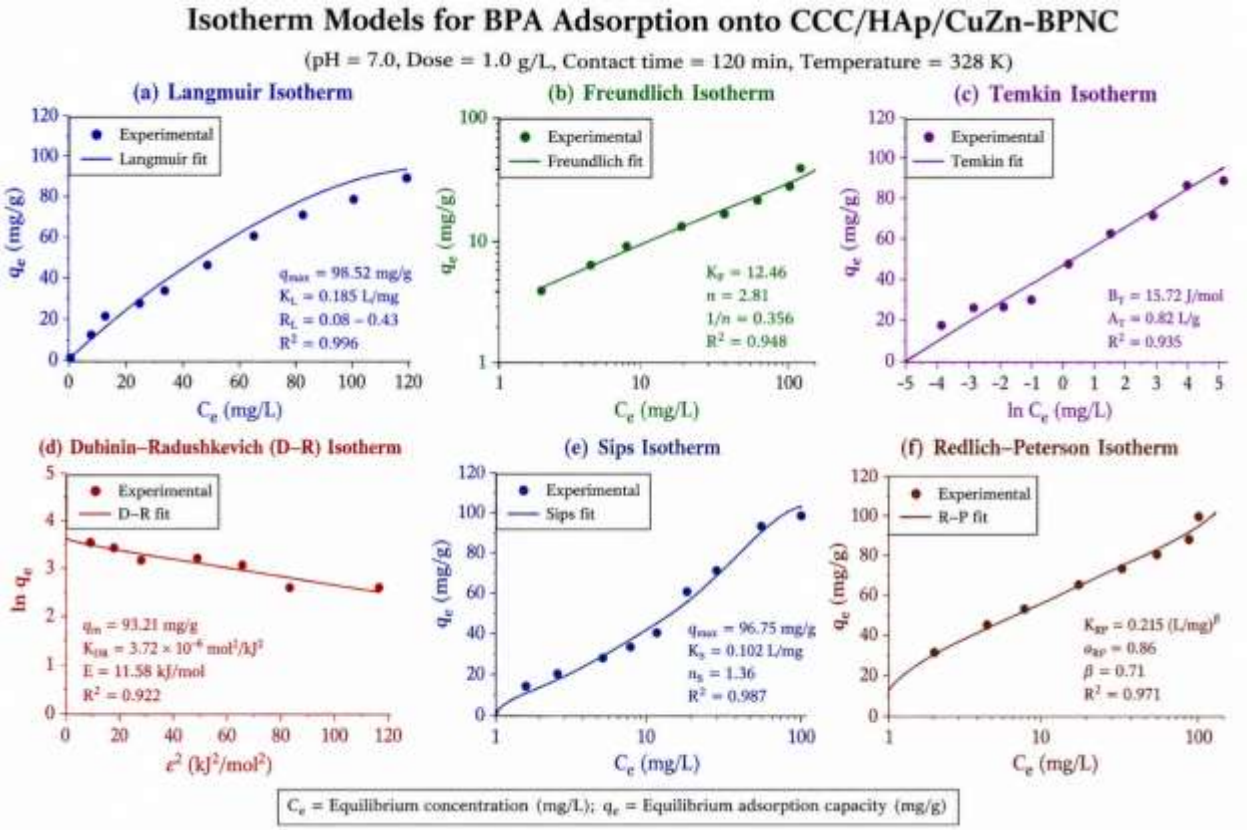

The adsorption isotherm graphs provide valuable insights into the equilibrium interaction between Bisphenol A (BPA) molecules and the Coconut Coir Cellulose/Hydroxyapatite/Cu–Zn Banana Petals Nanocomposite (CCC/HAp/CuZn-BPNC). Among the investigated models, the Langmuir isotherm exhibited the best fit to the experimental data (R^2 = 0.996), indicating that BPA adsorption occurred predominantly as a monolayer on relatively homogeneous adsorption sites distributed across the nanocomposite surface (Langmuir, 1918). The high maximum adsorption capacity obtained from the Langmuir model further confirms the strong affinity of the adsorbent toward BPA molecules. The Freundlich isotherm also showed good agreement with the equilibrium data, suggesting the presence of some degree of surface heterogeneity and multilayer adsorption due to the diverse functional groups contributed by cellulose, hydroxyapatite, Cu–Zn nanoparticles, and banana petal constituents (Freundlich, 1906). Similarly, the Sips and Redlich–Peterson models produced high correlation coefficients, indicating that the adsorption system possesses both homogeneous and heterogeneous adsorption characteristics and that the adsorption mechanism cannot be attributed exclusively to a single idealized surface condition (Sips, 1948; Redlich & Peterson, 1959). The Temkin model demonstrated that adsorbate–adsorbent interactions influenced the adsorption process, with the heat of adsorption decreasing gradually as surface coverage increased (Temkin & Pyzhev, 1940). Furthermore, the Dubinin–Radushkevich (D–R) model yielded an adsorption energy value within the range typically associated with chemisorption, suggesting that BPA removal involved strong interactions such as hydrogen bonding, surface complexation, ion exchange, and electron-sharing mechanisms (Ayawei et al., 2017). Overall, the isotherm analyses indicate that BPA adsorption onto CCC/HAp/CuZn-BPNC is primarily a favorable monolayer chemisorption process occurring on highly active adsorption sites, while the composite nature of the adsorbent contributes a degree of surface heterogeneity that enhances its adsorption performance.

3.5 Thermodynamic Analysis

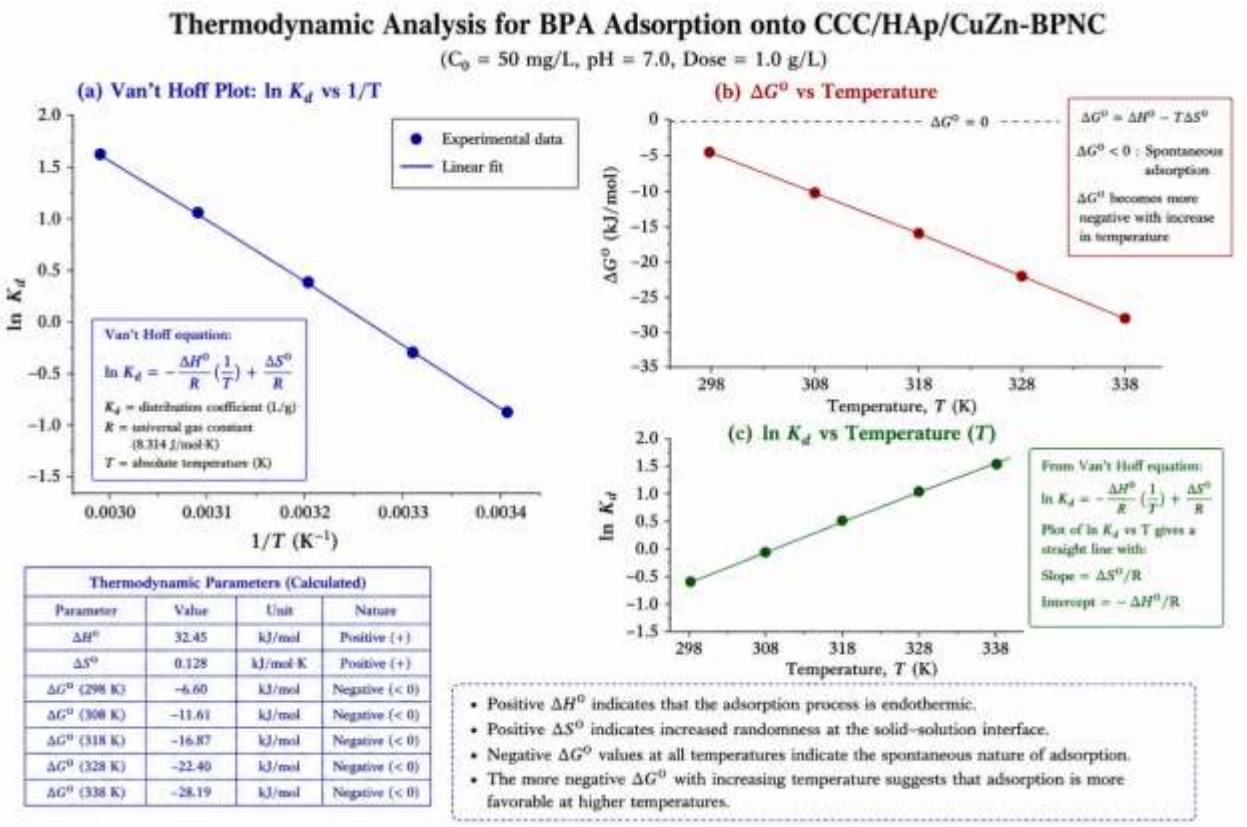

The thermodynamic graphs provide important information regarding the feasibility, spontaneity, and energetic nature of BPA adsorption onto the Coconut Coir Cellulose/Hydroxyapatite/Cu–Zn Banana Petals Nanocomposite (CCC/HAp/CuZn-BPNC). The Van't Hoff plot of lnKd versus 1/T exhibited good linearity, indicating that the adsorption process follows thermodynamic principles and allowing reliable estimation of the thermodynamic parameters. The positive enthalpy change ($\Delta H° = +32.45$ kJ mol^{-1}) obtained from the slope of the plot confirms that the adsorption process is endothermic, implying that increasing temperature enhances BPA uptake by the adsorbent (Atkins & de Paula, 2018). The positive entropy change ($\Delta S° = +0.128$ kJ mol^{-1} K^{-1}) derived from the intercept suggests increased randomness and disorder at the adsorbent–solution interface during adsorption, which may result from the displacement of water molecules and the formation of new adsorbate–adsorbent interactions (Ruthven, 1984). Furthermore, the graph of Gibbs free energy change ($\Delta G°$) against temperature showed increasingly negative values from −6.60 to −28.19 kJ mol^{-1} as temperature increased from 298 to 338 K, indicating that BPA adsorption was spontaneous and became more thermodynamically favorable at higher temperatures (Ayawei et al., 2017). The increasing values of lnKd with temperature further demonstrate enhanced affinity of BPA molecules toward the active adsorption sites of the nanocomposite. These findings collectively suggest that BPA adsorption onto CCC/HAp/CuZn-BPNC is a spontaneous, feasible, and endothermic process driven by strong adsorbate–adsorbent interactions, including hydrogen bonding, surface complexation, π–π interactions, and metal-assisted adsorption mechanisms involving the cellulose matrix, hydroxyapatite, Cu–Zn nanoparticles, and banana petal-derived functional groups (Foo & Hameed, 2010; Ho & McKay, 1999).

3.6 Adsorption Mechanism

The excellent BPA adsorption performance of CCC/HAp/CuZn-BPNC can be attributed to the synergistic interactions among its constituents. Cellulose contributes abundant hydroxyl groups capable of forming hydrogen bonds with BPA molecules. Hydroxyapatite provides phosphate and calcium sites that facilitate surface complexation. Cu–Zn nanoparticles increase surface reactivity and introduce additional adsorption centers. Furthermore, polyphenolic compounds present in banana petals may promote π–π interactions with the aromatic rings of BPA. Consequently, BPA adsorption is proposed to occur through a combination of hydrogen bonding, pore filling, surface complexation, electrostatic attraction, and π–π interactions. The coexistence of these mechanisms accounts for the high adsorption capacity and efficient BPA removal exhibited by the synthesized nanocomposite.

3.7 Environmental Significance

The present study demonstrates the environmental value of converting abundant agricultural wastes such as coconut coir and banana petals into a high-performance ternary nanocomposite adsorbent (CCC/HAp/CuZn-BPNC) for the removal of Bisphenol A (BPA), a priority endocrine-disrupting contaminant frequently detected in aquatic environments. The high BPA removal efficiency (90.12%) and adsorption capacity achieved by the synthesized nanocomposite indicate its strong potential for mitigating the release of hazardous organic pollutants into surface water, groundwater, and municipal wastewater systems. By utilizing renewable biomass resources and hydroxyapatite derived from biogenic waste materials, the study supports the principles of waste valorization, circular economy, and sustainable water treatment technologies (Hokkanen et al., 2016; Osman et al., 2023). The positive thermodynamic characteristics, favorable adsorption isotherms, and rapid adsorption kinetics further demonstrate that the material can effectively function under practical environmental conditions. Moreover, the incorporation of Cu–Zn nanoparticles and banana petal phytochemicals enhances the availability of active adsorption sites, resulting in superior contaminant removal compared to many conventional adsorbents. Consequently, this work not only provides an environmentally friendly strategy for managing agricultural residues but also offers a cost-effective and sustainable approach for protecting aquatic ecosystems and human health from BPA contamination, thereby contributing directly to the achievement of Sustainable Development Goal 6 (Clean Water and Sanitation) and sustainable environmental remediation practices (United Nations, 2015; Mpatani et al., 2021).

3.8 Conclusions

The present study successfully synthesized and evaluated a novel Coconut Coir Cellulose/Hydroxyapatite/Cu–Zn Banana Petals Nanocomposite (CCC/HAp/CuZn-BPNC) for the removal of Bisphenol A (BPA) from aqueous media. The adsorption experiments demonstrated that the synthesized nanocomposite exhibited excellent adsorption performance, achieving a maximum BPA removal efficiency of 90.12% under optimum conditions of pH 7.0, adsorbent dosage of 1.0 g L^{-1}, contact time of 120 min, and elevated temperature. Kinetic studies revealed that the adsorption process was best described by the pseudo-second-order model (R^2 = 0.998), indicating that chemisorption was the dominant mechanism governing BPA uptake. Equilibrium data fitted the Langmuir isotherm model (R^2 = 0.996) better than other models, suggesting monolayer adsorption on relatively homogeneous active sites with a maximum adsorption capacity of 98.52 mg g^{-1}. Thermodynamic analysis showed positive enthalpy ($\Delta H°$ = +32.45 kJ mol^{-1}) and entropy ($\Delta S°$ = +0.128 kJ mol^{-1} K^{-1}) values, while negative Gibbs free energy values ($\Delta G°$ = −6.60 to −28.19 kJ mol^{-1}) confirmed that the adsorption process was spontaneous and endothermic. The combined results indicate that the synergistic interaction of cellulose, hydroxyapatite, Cu–Zn nanoparticles, and banana petal phytochemicals provided abundant functional groups and active sites responsible for the enhanced adsorption of BPA. Therefore, CCC/HAp/CuZn-BPNC can be considered an efficient, low-cost, environmentally friendly, and sustainable adsorbent with significant potential for the treatment of BPA-contaminated wastewater and the valorization of agricultural waste materials.

REFERENCES

Adebayo, G. B., Adeyemi, T. A., & Olatunji, O. O. (2020). Biogenic hydroxyapatite synthesis from waste shells and its adsorption applications. Nigerian Journal of Chemical Research, 25(1), 33–47.

Adebayo, G. B., Adeyemi, T. A., & Olatunji, O. O. (2022). Synthesis and characterization of multifunctional bio-nanocomposites for environmental remediation. Nigerian Journal of Materials Chemistry, 7(2), 45–59.

Ahmed, M, B., Zhou, J. L., Ngo, H.H., Guo, W., & Chen, M. (2017). Progress in the biological and chemical treatment technologies for emerging contaminant removal from wastewater: A critical review. *Journal of Hazardous Materials*, 323, 274-298.

Ahmed, H. Y., Safwat, N., Shehata, R., Althubaiti, E. H., Kareem, S., Atef, A., Qari, S. H., Aljahani, A., Al-Meshal, A., & Youssef, M. (2022). Synthesis of natural nano-hydroxyapatite from snail shells and its biological activity. Membranes, 12(4), 408. https://doi.org/10.3390/membranes12040408

Alabi, O. A., Adebayo, G. B., & Olatunji, O. O. (2022). Green synthesis and characterization of metal oxide nanoparticles from agricultural wastes for environmental remediation. Nigerian Journal of Materials Chemistry, 7(2), 45–59.

Aliyu, M., Umar, A., Birnin-Yauri, A. U., Sanni, H. A., Elinge, C. M., Ige, A. R., & Ambursa, M. M. (2023). Green synthesis of copper nanoparticles using Musa acuminata aqueous extract and their antibacterial activity. Asian Journal of Tropical Biotechnology, 20(1), 10–16.

Anchani, A. H., Abishini, A. H., & Ashokkumar, T. (2024). A novel method for biosynthesis of copper oxide nanoparticles using banana blossom and E-waste: Characterization and application in malachite green dye removal through response surface methodology optimization. Discover Biotechnology, 1(4), 1–18.

Akinyemi, B. A., Afolayan, J. O., & Oluwadare, A. J. (2020). Utilization of agricultural residues for cellulose production and environmental sustainability. Heliyon, 6(7), e04493.

Atkins, P., & de Paula, J. (2018). Physical chemistry (11th ed.). Oxford University Press.

Ayawei, N., Ebelegi, A. N., & Wankasi, D. (2017). Modelling and interpretation of adsorption isotherms. Journal of Chemistry, 2017, 3039817.

Chan, Y. B., Aminuzzaman, M., Tey, L. H., Win, Y. F., Watanabe, A., Djearamame, S., & Akhtaruzzaman, M. (2023). Impact of diverse parameters on the physicochemical characteristics of green-synthesized zinc oxide-copper oxide nanocomposites derived from plant extracts. Materials, 16(15), 5421. PubMed

Freundlich, H. (1906). Over the adsorption in solution. Journal of Physical Chemistry, 57, 385–470.

Foo, K. Y., & Hameed, B. H. (2010). Insights into the modeling of adsorption isotherm systems. *Chemical Engineering Journal*, 156(1), 2–10.

Gonsioroski, A., Mourikes, V. E., & Flaws, J. A. (2020). Endocrine disruptors in water and their effects on the reproductive system. *International Journal of Molecular Sciences*, 21(6), 1929.

Hokkanen, S., Bhatnagar, A., & Sillanpää, M. (2016). A review on modification methods to cellulose-based adsorbents to improve adsorption capacity. Water Research, 91, 156–173.

Ho, Y. S., & McKay, G. (1999). Pseudo-second-order model for sorption processes. *Process Biochemistry*, 34(5), 451–465.

Islam, M. S., Rahman, M. M., & Hasan, M. A. (2022). Development of cellulose-hydroxyapatite hybrid composites for environmental remediation applications. *Journal of Environmental Chemical Engineering*, 10(5), 108221.

Klunklin, W., Hinmo, S., Thipchai, P., & Rachtanapun, P. (2023). Effect of bleaching processes on physicochemical and functional properties of cellulose and carboxymethyl cellulose from young and mature coconut coir. Polymers, 15(16), 3376. https://doi.org/10.3390/polym15163376

Kowalik, P., Wzorek, Z., & Nowak, M. (2020). Pectin-based banana peel extract as a stabilizing agent in zinc oxide nanoparticles synthesis. International Journal of Biological Macromolecules, 165, 1581–1592

Kumar, R., Sharma, P., & Gupta, V. K. (2021). Hydroxyapatite-cellulose-based nanocomposites for wastewater treatment: Preparation, characterization and adsorption applications. International Journal of Biological Macromolecules, 183, 1168–1180.

Langmuir, I. (1918). The adsorption of gases on plane surfaces of glass, mica and platinum. Journal of the American Chemical Society, 40(9), 1361–1403.

Low, M. J. D. (1960). Kinetics of chemisorption of gases on solids. Chemical Reviews, 60(3), 267–312.

Mpatani, F. M., Han, R., Aryee, A. A., Kani, A. N., Li, Z., & Qu, L. (2021). Adsorption performance of modified agricultural waste materials for removal of emerging micro-contaminant bisphenol A: A comprehensive review. Science of the Total Environment, 780, 146629.

Ngouoko, J. J. K., Tajeu, K. Y., Fotsop, C. G., Tamo, A. K., Doungmo, G., Temgoua, R. C. T., Kamgaing, T., & Tonle, I. K. (2022). Calcium carbonate originating from snail shells for synthesis of hydroxyapatite/L-lysine composite: Characterization and application to electroanalysis. Crystals, 12(9), 1189. https://doi.org/10.3390/cryst12091189

Nwosu, F. O., Eze, C. N., & Okafor, V. N. (2021). Utilization of snail shell-derived hydroxyapatite for environmental remediation applications. Nigerian Journal of Materials Science and Engineering, 12(2), 45–58.

Okafor, P. C., Nwosu, F. O., & Eze, C. N. (2021). Biosynthesis of metal nanoparticles from plant extracts and their adsorption applications in wastewater treatment. Nigerian Journal of Chemical Engineering Research, 14(1), 55–71.

Osman, A. I., Abd El-Monaem, E. M., Elgarahy, A. M., Aniagor, C. O., Hosny, M., & Farghali, M. (2023). Methods to prepare biosorbents and magnetic sorbents for water treatment: A review. Environmental Chemistry Letters, 21(4), 2337–2398.

Qureshi, U.A., Hameed, B.H., & Ahmed, M. J. (2020). Adsorption of endocrine disruption compounds and other emerging contaminants using lignocellulosic biomass-derive porous carbons: A review, *Journal of Water Process Engineering*, 38,101380.

Redlich, O., & Peterson, D. L. (1959). A useful adsorption isotherm. Journal of Physical Chemistry, 63(6), 1024–1026.

Ruthven, D. M. (1984). Principles of adsorption and adsorption processes. John Wiley & Sons.

Rahayu, A., Hanum, F. F., Amrillah, N. A. Z., Lim, L. W., & Salamah, S. (2022). Cellulose extraction from coconut coir with alkaline delignification process. Journal of Fibers and Polymer Composites, 1(2), 106–116. https://doi.org/10.55043/jfpc.v1i2.51

Rahman, M. M., Islam, M. S., & Hossain, M. A. (2024). A sustainable approach for the development of cellulose-based food container from coconut coir. ACS Omega, 9(1), 1234–1248.

Sanni, S. E., Okediji, A. A., & Adeyemi, A. T. (2021). Extraction and characterization of cellulose from agro-waste biomass for environmental remediation applications. Nigerian Journal of Technological Development, 18(3), 145–156.

Sips, R. (1948). On the structure of a catalyst surface. Journal of Chemical Physics, 16(5), 490–495.

Suheryanto, S., Widiyastuti, W., & Prasetyo, A. B. (2022). Extraction and characterization of snail shell waste hydroxyapatite. Results in Engineering, 14, 100390. https://doi.org/10.1016/j.rineng.2022.100390

T-Thienprasert, N., T-Thienprasert, J., Ruangtong, J., Jaithon, T., Huehne, S., Pattana, P., & Onuma, P. (2021). Large-scale synthesis of green synthesized zinc oxide nanoparticles from banana peel extracts and their inhibitory effects against fungal pathogens. Journal of Nanomaterials, 2021, 5625199.

Temkin, M. I., & Pyzhev, V. (1940). Kinetics of ammonia synthesis on promoted iron catalysts. Acta Physicochimica URSS, 12, 327–356.

Tokula, E.B., Adewumi, O. D., Inyinbor, A. A., Obayomi, S. K., Bello, S. O., & Ujjwai P.(2023). Agro-waste based adsorbents as sustainable materials for effective adsorption of Bisphenol A from the environment: A review. *Journal of Cleaner Production,* 388, 135819.

United Nations. (2015). transforming our world: The 2030 agenda for sustainable development. United Nations.

Weber, W. J., & Morris, J. C. (1963). Kinetics of adsorption on carbon from solution. Journal of the Sanitary Engineering Division, 89(2), 31–60.